Journal of Solid State Chemistry 182 (2009) 1935–1943

Contents lists available at ScienceDirect

Journal of Solid State Chemistry

journal homepage: www.elsevier.com/locate/jssc

Revised phase diagram of Li_2MoO_4–$ZnMoO_4$ system, crystal structure and crystal growth of lithium zinc molybdate

Sergey F. Solodovnikov [a,b,*], Zoya A. Solodovnikova [a], Evgeniya S. Zolotova [a], Lyudmila I. Yudanova [a], Tatyana Yu. Kardash [c], Anatoly A. Pavlyuk [a], Vladimir A. Nadolinny [a]

[a] Nikolaev Institute of Inorganic Chemistry, Siberian Branch, Russian Academy of Sciences, Acad. Lavrentiev Ave. 3, Novosibirsk 630090, Russia
[b] Novosibirsk State University, Pirogova St. 2, Novosibirsk 630090, Russia
[c] Boreskov Institute of Catalysis, Siberian Branch, Russian Academy of Sciences, Acad. Lavrentiev Ave. 5, Novosibirsk 630090, Russia

ARTICLE INFO

Article history:
Received 17 March 2009
Received in revised form
28 April 2009
Accepted 30 April 2009
Available online 10 May 2009

Keywords:
Lithium zinc molybdate
T–x phase diagram
Nonstoichiometry
Crystal structure
Cation disorder
Crystal growth
Physical properties

ABSTRACT

Orthorhombic lithium zinc molybdate was first chosen and explored as a candidate for double beta decay experiments with ^{100}Mo. The phase equilibria in the system Li_2MoO_4–$ZnMoO_4$ were reinvestigated, the intermediate compound $Li_2Zn_2(MoO_4)_3$ of the α-$Cu_3Fe_4(VO_4)_6$ (lyonsite) type was found to be nonstoichiometric: $Li_{2-2x}Zn_{2+x}(MoO_4)_3$ ($0 \le x \le 0.28$) at 600 °C. The eutectic point corresponds to 650 °C and 23 mol% $ZnMoO_4$, the peritectic point is at 885 °C and 67 mol% $ZnMoO_4$. Single crystals of the compound were prepared by spontaneous crystallization from the melts and fluxes. In the structures of four $Li_{2-2x}Zn_{2+x}(MoO_4)_3$ crystals ($x = 0$; 0.03; 0.21; 0.23), the cationic sites in the face-shared octahedral columns were found to be partially filled and responsible for the compound nonstoichiometry. It was first showed that with increasing the *x* value and the number of vacancies in *M*3 site, the average *M*3–O distance grows and the lithium content in this site decreases almost linearly. Using the low-thermal-gradient Czochralski technique, optically homogeneous large crystals of lithium zinc molybdate were grown and their optical, luminescent and scintillating properties were explored.

1. Introduction

Numerous tungstates and molybdates are well known in literature and have important properties and applications. For example, double tungstates and molybdates with the general formula $MRE(XO_4)_2$ (where M = alkali metal, RE = trivalent rare earth, and $X = W^{6+}$ or Mo^{6+}) are excellent *RE*-doped laser hosts [1]. Another prospective field for application of tungstates and molybdates is scintillating materials. Among these, we may call MWO_4 (M = Zn, Cd, Pb) [2] having good scintillating characteristics, chemical and radiation stability, high-density and high-effective atomic number, which are very important for detection of gamma radiation and high-energy elementary particles.

At present new facilities arise to use large crystals of tungstates and molybdates in experiments on search for neutrinoless double β decay ($0\nu2\beta$) [3]. Significant interest to this problem is connected with observed neutrino oscillations which strongly suggest that neutrinos have nonzero mass. ^{100}Mo is one of the most promising nucleus for 2β decay experiments because of its high transition energy $Q_{2\beta} = 3035$ keV [4]. Thus, single crystals of molybdates may be perspective detector materials for these experiments. Oxide crystals for high-sensitive cryogenic bolometric detectors of 2β decay should meet the following requirements: high-light output and transparency, fast response, radiopurity, maximal content of the element under study (Mo in our case), and diamagnetic properties for reaching low temperatures of measurements. In addition, low-density and low-effective atomic number are desirable to minimize γ background. However, a few tested crystals of simple molybdates such as $MMoO_4$ (M = Pb, Mg, Ca, Cd, Zn) [5–7], Li_2MoO_4 [8] have some disadvantages (presence of natural radioactive impurities, high-effective *Z* value, low-light output and so on). Therefore, search for new and more effective molybdate crystals for this application is of great interest.

A possible field for the search could be, in particular, double molybdates of relatively light metals. As a candidate for developing a possible detector material for double beta decay experiments with ^{100}Mo we first chose orthorhombic $Li_2Zn_2(MoO_4)_3$. The compound contains 46.09% by weight of molybdenum and has no radioactive and heavy elements. In addition, such substance could also be used for detecting double beta decay of ^{64}Zn and ^{70}Zn.

Lithium zinc molybdate was first obtained by Demyanets [9] as a by-product of hydrothermal crystallization of $ZnMoO_4$ from LiCl

* Corresponding author at: Nikolaev Institute of Inorganic Chemistry, Siberian Branch, Russian Academy of Sciences, Acad. Lavrentiev Ave. 3, Novosibirsk 630090, Russia. Fax: +7 383 3309489.
E-mail address: solod@che.nsk.su (S.F. Solodovnikov).

0022-4596/$ - see front matter © 2009 Elsevier Inc. All rights reserved.
doi:10.1016/j.jssc.2009.04.036

containing aqueous solutions. Later, stoichiometric $Li_2Zn_2(MoO_4)_3$ was prepared by solid-state synthesis and crystallization from the melts and characterized in detail [10–14]. Efremov and Trunov have studied T–x phase diagram of the Li_2MoO_4–$ZnMoO_4$ system [12] and found that $Li_2Zn_2(MoO_4)_3$ is the single intermediate compound, which exhibits no phase transitions and melts incongruently at 925 °C. Lithium zinc molybdate along with isostructural $Li_2M_2(MoO_4)_3$ (M = Fe, Ni, Mn, Cu, Co, Mg) [15–20] belong to the numerous structural family of lyonsite α-$Cu_3Fe_4(VO_4)_6$ [21,22]. Quite recently, Xue et al. explored subsolidus phase relations in the system ZnO–Li_2O–MoO_3, determined the crystal structure of $Li_2Zn_2(MoO_4)_3$ using X-ray powder diffraction data and grew $Li_2Zn_2(MoO_4)_3$ single crystals with dimensions up to $10\times4\times3\ mm^3$ by top-seeded solution growth technique [23–25].

It should be noted that the latter authors have found lithium zinc molybdate to be nonstoichiometric, $Li_{2-2x}Zn_{2+x}(MoO_4)_3$ ($-0.1\le x\le0.3$) [25]. This fact confirms our preliminary data on lithium zinc molybdate [26,27] and gives a new evidence for a probable departure of $Li_2M_2(MoO_4)_3$ from stoichiometry that have been escaping attention of researchers for a long time in spite of existing nonstoichiometric lyonsite-type phases such as $Na_{2-2x}M_{2+x}(MoO_4)_3$ (M = Co, Ni, Cu, Zn) [10,13,28], $(Cu,M^{2+})_{4-x}Mo_3O_{12}$ (M = Cu, Zn, Co, Fe, Mn) [29–34], and others [22]. The reason for such departures from stoichiometry are connected with close ionic radii of A^+ and M^{2+} that facilitates heterovalent substitution/subtraction following the scheme $2A^+\rightarrow M^{2+}+\square$ where $A^+=Li^+$, Na^+, Cu^+, and $\square$ is a cationic vacancy [13,17]. The first unequivocal evidence of nonstoichiometry of double molybdates of lithium and bivalent metals resulting in the general formula $Li_{2-2x}M_{2+x}(MoO_4)_3$ was obtained by us for lithium manganese molybdate [17] that was confirmed later by Sebastian et al. [20] for lithium magnesium molybdate.

The purpose of our work was a detailed research of thermal stability, structure and properties required for developing technology for growth of large single crystals of $Li_{2-2x}Zn_{2+x}(MoO_4)_3$, which is complicated by both its incongruent melting and nonstoichiometry. Herein we present the results on studying T–x phase diagram of the Li_2MoO_4–$ZnMoO_4$ system, the homogeneity range and the crystal structure of lithium zinc molybdate. Based on these data, we also grew large crystals of lithium zinc molybdate with a nearly stoichiometric composition and performed preliminary measurements of optical, luminescent and scintillating properties of the compound. We suppose that our data are important for developing growth technologies of $Li_{2-2x}M_{2+x}(MoO_4)_3$ (M = Mg, Mn, Co, Ni, Cu, Zn) and related crystals and hope that these results could also elucidate the details of the crystal chemistry of double molybdates and other compounds belonging to the lyonsite-type.

2. Experimental

2.1. Synthesis and crystallization

As starting reagents commercially available molybdates Li_2MoO_4 and $ZnMoO_4$ (both >99.9%) were taken. The reagents were calcined at 500 °C for 5 h to remove moisture traces. The powder diffraction patterns of as-prepared anhydrous molybdates agree well with literature data of ICDD PDF-2. The samples for studying phase relations and constructing T–x phase diagrams of the system Li_2MoO_4–$ZnMoO_4$ were prepared by solid-state reactions from $ZnMoO_4$ and Li_2MoO_4 with the step of 5–10 mol% (in the homogeneity region of lithium zinc molybdate the step was 1–2 mol% and less) at 550 °C for 120 h and at 575 °C for 200 h with intermediate grindings in a day. In order to determine the homogeneity range of the double molybdate with X-ray diffraction analysis, mixtures of the components corresponding to nominal compositions $Li_{2-2x}M_{2+x}(MoO_4)_3$ with $x=-0.15$–0.35 ($\Delta x=0.05$) were prepared. The samples were sintered at 500, 550 and 600 °C for 50, 50 and 150 h, respectively, and then quenched in air.

Small crystals of lithium zinc molybdate were grown by spontaneous crystallization of molten ceramic samples or mixtures of different compositions including samples of the ternary system Li_2MoO_4–K_2MoO_4–$ZnMoO_4$. As fluxes Li_2MoO_4, lithium polymolybdates and $K_2Mo_2O_7$ were used. The ground mixtures were put in platinum crucibles with platinum lids and heated to 550–1000 °C. After holding at these temperatures for a day, the melts then were cooled to 500 °C at rates of 3–5 °C h^{-1} and finally cooled down to room-temperature in a switched-off furnace. The temperature and the cooling rates were controlled and kept automatically with an accuracy of ±0.5°.

Large crystals of lithium zinc molybdate were grown from a platinum crucible of 70 mm in diameter and 120 mm in height using low-thermal-gradient Czochralski technique [35]. The crystals were grown from molten mixtures of Li_2CO_3, MoO_3 and ZnO (all 3–4N purity grade) with 10–15 mol% excess of Li_2CO_3 and MoO_3 compared with the stoichiometric composition. In some crystallization experiments, the additionally purified molybdenum trioxide was used. The pulling rate of a seed on [100] was about 0.5 mm h^{-1}.

2.2. X-ray diffraction and structure determination

Monitoring of solid-state synthesis and phase equilibration were carried out by X-ray powder diffraction (XRD) with a DRON-3M or URD-6 diffractometers using Ni-filtered Cu$K\alpha$ radiation. Powder patterns of samples from the homogeneity range of lithium zinc molybdate were taken on a Thermo ARL X'tra diffractometer equipped with a θ–θ goniometer and a Si(Li) Peltier cooled detector. Silicon powder ($a=5.43075(5)$ Å) was used as an internal standard for each sample. Data were collected over the range of $5\le2\theta\le90°$ with a 0.02° step and a counting time 5 s per step. The lattice parameters were refined by model-based Le Bail fitting with the GSAS program package with EXPGUI user interface [36]. The homogeneity range limits were determined from the dependence of the unit cell parameters on the sample compositions (Table 1). The X-ray powder diffraction patterns of ground crystals of lithium zinc molybdate prepared by spontaneous crystallization were consistent with the calculated X-ray powder diffraction pattern, experimental XRD data for corresponding sintered samples and the powder pattern reported for $Li_2Zn_2(MoO_4)_3$ [11] (ICDD PDF no. 26-1209).

Four crystals of lithium zinc molybdate taken for structure determination were obtained from melts and molten mixtures of the following compositions: **I**—$Li_2Zn_2(MoO_4)_3$; **II**—$Li_2MoO_4+2ZnMoO_4+0.5Li_2Mo_2O_7$; **III**—$Li_2MoO_4+3K_2MoO_4+4ZnMoO_4+2K_2Mo_2O_7$; **IV**—$Li_{1.5}Zn_{2.25}(MoO_4)_3$. Single-crystal X-ray diffraction data for structure determinations were collected with graphite-monochromated Mo$K\alpha$ radiation ($\lambda=0.71073$ Å) on a Bruker-Nonius X8 Apex CCD area-detector diffractometer at room temperature using φ-scans. Processing of the data was accomplished using SAINT program; an absorption correction was applied with SADABS program [37]. The structures were solved and refined by full-matrix least-squares method on F^2 in anisotropic approximation with SHELX-97 package [38]. Results of the data collection and structure determinations are given in Table 2.

The structure solutions of these four crystal samples were performed proceeding from their isostructurality to $Li_{1.60}Mn_{2.20}(MoO_4)_3$ [17]. For all the crystals studied the systematic absences

Table 1
Crystallographic data for solid solutions $Li_{2-2x}Zn_{2+x}(MoO_4)_3$ quenched from 600 °C.

Composition of sample	Unit cell parameters			V (Å^3)	Calculated density (g cm^{-3})
	a (Å)	b (Å)	c (Å)		
$Li_{2.2}Zn_{1.9}(MoO_4)_3$[a]	5.1167(2)	10.4948(3)	17.6234(7)	946.35(6)	–
$Li_{2.1}Zn_{1.95}(MoO_4)_3$[a]	5.1169(2)	10.4950(3)	17.6215(6)	946.31(6)	–
$Li_{2.0}Zn_{2.0}(MoO_4)_3$	5.1162(2)	10.4962(4)	17.6241(6)	946.43(6)	4.382[b]
$Li_{1.9}Zn_{2.05}(MoO_4)_3$	5.1067(2)	10.5048(4)	17.6446(6)	946.54(6)	4.400
$Li_{1.8}Zn_{2.1}(MoO_4)_3$	5.0982(1)	10.5159(2)	17.6671(4)	947.17(5)	4.415
$Li_{1.7}Zn_{2.15}(MoO_4)_3$	5.0900(1)	10.5277(2)	17.6900(5)	947.94(4)	4.430
$Li_{1.6}Zn_{2.2}(MoO_4)_3$	5.0812(1)	10.5362(3)	17.7072(5)	947.98(4)	4.447
$Li_{1.5}Zn_{2.25}(MoO_4)_3$	5.0731(1)	10.5465(3)	17.7247(5)	948.33(4)	4.464
$Li_{1.4}Zn_{2.3}(MoO_4)_3$[c]	5.0675(1)	10.5536(3)	17.7358(5)	948.52(4)	–
$Li_{1.3}Zn_{2.35}(MoO_4)_3$[c]	5.0681(1)	10.5532(3)	17.7344(5)	948.52(4)	–

[a] There is Li_2MoO_4 impurity in the sample.
[b] Measured density is 4.38 ± 0.02 g cm^{-3}.
[c] There is $ZnMoO_4$ impurity in the sample.

Table 2
Crystal data and structure refinement details for $Li_{2-2x}Zn_{2+x}(MoO_4)_3$ ($x = 0$, 0.03, 0.21 and 0.23).

Formula	$Li_2Zn_2(MoO_4)_3$ (**I**)	$Li_{1.93}Zn_{2.03}(MoO_4)_3$ (**II**)	$Li_{1.58}Zn_{2.21}(MoO_4)_3$ (**III**)	$Li_{1.55}Zn_{2.23}(MoO_4)_3$ (**IV**)
Formula weight (g/mol)	624.44	626.10	635.13	636.15
Crystal system	Orthorhombic	Orthorhombic	Orthorhombic	Orthorhombic
Space group	*Pnma*	*Pnma*	*Pnma*	*Pnma*
Unit cell dimensions (Å)	$a = 5.1139(5)$, $b = 10.4926(13)$, $c = 17.645(2)$	$a = 5.1100(2)$ $b = 10.5070(6)$, $c = 17.6474(10)$	$a = 5.0819(1)$, $b = 10.5387(2)$, $c = 17.7077(3)$	$a = 5.0790(1)$, $b = 10.5421(2)$, $c = 17.7161(3)$
V (Å^3); Z	946.80(18)/4	947.50(8)/4	948.37(3)/4	948.58(3)/4
Calculated density (g cm^{-3})	4.381[a]	4.389	4.448	4.454
Crystal size (mm)	$0.12 \times 0.04 \times 0.03$	$0.10 \times 0.02 \times 0.01$	$0.10 \times 0.07 \times 0.06$	$0.09 \times 0.02 \times 0.03$
μ(Mo$K\alpha$) (mm^{-1})	8.921	8.994	9.418	9.465
θ Range (deg) for data collection	2.26–32.59	2.26–32.59	2.25–36.31	2.25–30.53
Miller index ranges	$-7 \le h \le 3$, $-15 \le k \le 6$, $-26 \le l \le 25$	$-4 \le h \le 7$, $-14 \le k \le 15$, $-26 \le l \le 25$	$-7 \le h \le 8$, $-16 \le k \le 17$, $-14 \le l \le 28$	$-4 \le h \le 7$, $-15 \le k \le 14$, $-25 \le l \le 24$
Reflections collected/unique	4583/1761 [R(int) = 0.0473]	9277/1806 [R(int) = 0.0360]	11190/2392 [R(int) = 0.0233]	8336/1525 [R(int) = 0.0307]
No. of variables	98	99	99	99
Goodness-of-fit on F^2 (GOF)	1.000	1.051	1.082	1.209
Final R indices [$I > 2\sigma(I)$]	$R(F) = 0.0372$, w$R(F^2) = 0.0831$	$R(F) = 0.0227$, w$R(F^2) = 0.0490$	$R(F) = 0.0188$, w$R(F^2) = 0.0418$	$R(F = 0.0186$, w$R(F^2) = 0.0431$
R indices (all data)	$R(F) = 0.0540$, w$R(F^2) = 0.0895$	$R(F) = 0.0272$, w$R(F^2) = 0.0506$	$R(F) = 0.0223$, w$R(F^2) = 0.0430$	$R(F) = 0.0190$, w$R(F^2) = 0.0433$
Extinction coefficient	0.0002(2)	0.00078(14)	0.00274(14)	0.0095(3)
Largest difference peak/hole (e Å^{-3})	2.929/−1.805	1.330/−0.975	1.591/−2.465	0.682/−2.180

[a] Measured density of a sintered sample is 4.38 g cm^{-3}.

of reflections (hkl: $h = 2n$, $0kl$: $k+l = 2n$) correspond to the space group *Pnma* found for lithium manganese molybdate. Thus, for solving the structure of lithium zinc molybdate, the coordinates of the 2Mo and 3Mn atoms from [17] were taken as the starting structure model. The positions of seven independent oxygen atoms were revealed from difference electron density maps. In accordance with Ozima et al. [16], a crystal chemical formula of lithium zinc molybdate should be written as $(M1)(M2)_2(M3)(MoO_4)_3$ where the lithium and zinc atoms are distributed over the $M1$, $M2$ and $M3$ sites. However, after isotropic refinement of these atomic positions with fully occupied and independently varied populations of Li and Zn, we found that the resulting zinc contents in the unit cells of **II**, **III** and **IV** were greater than the total lithium content, even taking into account possible errors. Thus, further solutions of all four structures was carried out according to the common scheme taking into consideration both statistical distribution of the Li^+ and Zn^{2+} cations over three crystallographic positions $M1$, $M2$ and $M3$ and possible nonstoichiometry of lithium zinc molybdate. This required a cation position of $M1$, $M2$ and $M3$ sites to be partially deficient. As such a position, $M3$ site was chosen because the analogous sites are partly occupied in the structurally similar and nonstoichiometric compounds such as (Cu, $M^{2+})_{4-x}Mo_3O_{12}$ (M = Cu, Zn, Co, Fe, Mn) [29–34], $Zn_{3.77}V_{1.54}Mo_{1.46}O_{12}$ [39] and other related compounds of the lyonsite-type [22]. After taking $M1$ and $M2$ sites as fully occupied and $M3$ site as partly deficient, the general crystal chemical formula of lithium zinc molybdate adopts the form $(Li_{1-x}Zn_x)(Li_{1-y}Zn_y)_2(Li_zZn_t\square_{1-z-t})(MoO_4)_3$ and, with keeping the electrical neutrality condition, we obtain the following relation between the x, y, z and t parameters: $x+2y+z+2t = 3$. Anisotropic refinement with this constraint performed for all four crystals allowed us to find the populations x, y, z and t for the $M1$, $M2$ and $M3$ sites. The final positional and equivalent isotropic displacement parameters of $Li_{2-2x}Zn_{2+x}(MoO_4)_3$ with $x = 0$(**I**); 0.03(**II**); 0.21(**III**) and 0.23(**IV**) are listed in Table 3. Selected interatomic distances are given in Table 4 and results of calculations of bond valence sums using data of [40] are summarized in Table 5. Further details of the crystal structure investigations can be

Table 3
Positional and equivalent isotropic displacement parameters for $Li_{2-2x}Zn_{2+x}(MoO_4)_3$ ($x = 0$, 0.03, 0.21 and 0.23).[a]

Atom	Population	x	y	z	U_{eq} (Å^2)[b]
Mo(1)	Mo	0.27824(9)	0.25	0.44306(3)	0.00707(12)
		0.27857(6)		0.44317(2)	0.00835(7)
		0.27779(4)		0.44371(1)	0.00861(4)
		0.27758(5)		0.44375(1)	0.00888(7)
Mo(2)	Mo	0.77643(7)	0.52677(4)	0.34343(2)	0.00817(11)
		0.77671(4)	0.52677(2)	0.34347(1)	0.00936(6)
		0.77637(3)	0.52729(1)	0.34373(1)	0.00968(4)
		0.77632(3)	0.52735(2)	0.34374(1)	0.00996(7)
M(1)	0.797(2)Li+0.203(2)Zn	0.2445(5)	0.75	0.30201(18)	0.0133(7)
	0.801(2)Li+0.199(2)Zn	0.2445(3)		0.30214(10)	0.0135(5)
	0.813(2)Li+0.187(2)Zn	0.2436(2)		0.30235(7)	0.0138(3)
	0.816(2)Li+0.184(2)Zn	0.2434(3)		0.30225(9)	0.0143(5)
M(2)	0.284(2)Li+0.716(2)Zn	0.25466(13)	0.57863(7)	0.47097(4)	0.01007(18)
	0.281(2)Li+0.719(2)Zn	0.25460(8)	0.57871(4)	0.47103(2)	0.01128(12)
	0.275(1)Li+0.725(1)Zn	0.25481(5)	0.57872(3)	0.47098(2)	0.01102(8)
	0.270(2)Li+0.730(2)Zn	0.25488(6)	0.57874(3)	0.47095(2)	0.01143(12)
M(3)	0.635(3)Li+0.365(3)Zn	0.6052(4)	0.25	0.24916(10)	0.0107(5)
	0.570(7)Li+0.396(3)Zn+0.034□	0.6060(2)		0.24901(6)	0.0152(3)
	0.223(5)Li+0.570(2)Zn+0.207□	0.6072(2)		0.24909(4)	0.0345(3)
	0.190(6)Li+0.582(2)Zn+0.228□	0.6076(2)		0.24914(4)	0.0354(3)
O(1)	O	0.3599(9)	0.25	0.3470(2)	0.0124(9)
		0.3603(5)		0.34700(14)	0.0134(5)
		0.3627(4)		0.34832(10)	0.0152(3)
		0.3628(5)		0.34845(12)	0.0158(4)
O(2)	O	0.5561(9)	0.25	0.5067(3)	0.0109(9)
		0.5557(5)		0.50683(15)	0.0131(5)
		0.5553(4)		0.50738(10)	0.0130(3)
		0.5558(4)		0.50731(12)	0.0137(4)
O(3)	O	0.0810(6)	0.1158(3)	0.46267(18)	0.0130(6)
		0.0808(4)	0.11589(18)	0.46274(10)	0.0132(3)
		0.0794(3)	0.11606(13)	0.46290(7)	0.0134(2)
		0.0792(3)	0.11592(14)	0.46301(8)	0.0135(3)
O(4)	O	0.5829(6)	0.4893(3)	0.42480(18)	0.0123(6)
		0.5824(4)	0.48902(18)	0.42489(10)	0.0142(3)
		0.5820(3)	0.48931(12)	0.42508(7)	0.0135(2)
		0.5816(3)	0.48941(14)	0.42509(8)	0.0141(3)
O(5)	O	0.5777(7)	0.6234(3)	0.28707(19)	0.0167(7)
		0.5778(4)	0.6233(2)	0.28709(11)	0.0170(4)
		0.5773(3)	0.62357(14)	0.28720(8)	0.0178(3)
		0.5773(3)	0.62358(16)	0.28729(9)	0.0181(3)
O(6)	O	0.8541(6)	0.3847(3)	0.29512(18)	0.0115(6)
		0.8549(4)	0.38483(18)	0.29535(10)	0.0134(3)
		0.8565(3)	0.38629(13)	0.29584(7)	0.0156(2)
		0.8571(3)	0.38637(15)	0.29595(9)	0.0164(3)
O(7)	O	1.0588(6)	0.6136(3)	0.37292(19)	0.0139(6)
		1.0595(4)	0.61338(18)	0.37303(10)	0.0139(3)
		1.0599(3)	0.61397(13)	0.37298(7)	0.0145(2)
		1.0601(3)	0.61409(15)	0.37309(8)	0.0149(3)

[a] Correspond to the first, second, third and fourth lines for each atom, respectively.
[b] U_{eq} is defined as one third of the trace of the orthogonalized U_{ij} tensor.

obtained from the Fachinformationszentrum Karlsruhe, 76344 Eggenstein–Leopoldshafen, Germany, (fax: +49 7247 808 666; e-mail: crysdata@fiz.karlsruhe.de) on quoting the depository numbers CSD 380277, 380278, 380279 and 380280 for $Li_2Zn_2(MoO_4)_3$, $Li_{1.54}Zn_{2.23}(MoO_4)_3$, $Li_{1.59}Zn_{2.21}(MoO_4)_3$ and $Li_{1.93}Zn_{2.03}(MoO_4)_3$, respectively.

2.3. Thermal analysis and density measurements

For determining *T–x* phase diagram of the system Li_2MoO_4–$ZnMoO_4$ and thermal stability of lithium zinc molybdate, thermoanalytical study was carried out in air with a MOM Q-1500D derivatograph (Pt crucibles, Pt–Pt/Rh thermocouples, heating, cooling and DTA curves, Al_2O_3 as reference substance, heating and cooling rates 10 °C min^{-1}, accuracy of effect measuring ±10 °C).

The densities of some samples were determined pycnometrically in toluene at 20±0.1 °C. Estimated errors of density measurements are ±0.02 g cm^{-3}.

3. Results and discussion

3.1. T–x phase diagram and homogeneity range in the Li_2MoO_4–$ZnMoO_4$ system

The melting points of $ZnMoO_4$ and Li_2MoO_4 were found to be 705 and 1000 °C, respectively, which are in a good agreement with data of [12]. DTA curves and XRD data show no phase transitions of Li_2MoO_4 and $ZnMoO_4$ and absence of any notable mutual solubility of the components in the temperature region studied. *T–x* phase diagrams of the system Li_2MoO_4–$ZnMoO_4$ is presented in Fig. 1. The coordinates of the eutectic point in the system are

Table 4
Selected interatomic distances (Å) for $Li_{2-2x}Zn_{2+x}(MoO_4)_3$ ($x = 0$, 0.03, 0.21 and 0.23)[a].

$Mo(1)O_4$ tetrahedron		$Mo(2)O_4$ tetrahedron		$M(1)O_6$ trigonal prism	
Mo(1)–O(1)	1.746(4)	Mo(2)–O(5)	1.746(3)	M(1)–O(7)#1	2.125(4) × 2
	1.748(3)		1.7467(19)		2.126(2) × 2
	1.7435(18)		1.7479(14)		2.1191(16) × 2
	1.743(2)		1.7467(16)		2.1199(18) × 2
Mo(1)–O(3)	1.766(3) × 2	Mo(2)–O(6)	1.763(3)	M(1)–O(5)	2.177(4) × 2
	1.7680(19) × 2		1.7620(18)		2.178(2) × 2
	1.7676(13) × 2		1.7586(13)		2.1732(17) × 2
	1.7693(15) × 2		1.7589(15)		2.173(2) × 2
Mo(1)–O(2)	1.811(4)	Mo(2)–O(7)	1.785(3)	M(1)–O(5)#2	2.228(4) × 2
	1.807(3)		1.7857(18)		2.231(2) × 2
	1.8057(18)		1.7830(13)		2.2370(18) × 2
	1.806(2)		1.7845(15)		2.237(2) × 2
〈Mo(1)–O〉	1.772	Mo(2)–O(4)	1.787(3)	〈M(1)–O〉	2.177
	1.773		1.7910(19)		2.178
	1.771		1.7920(13)		2.176
	1.772		1.7931(15)		2.177
		〈Mo(2)–O〉	1.770		
			1.771		
			1.770		
			1.771		
$M(2)O_6$ octahedron		$M(3)O_6$ octahedron		Shortest metal-metal distances	
M(2)–O(7)#1	2.033(3)	M(3)–O(6)#2	2.063(3) × 2	Mo(1)–M(2)#3	3.3526(8)
	2.0291(19)		2.066(2) × 2		3.3500(5)
	2.0324(13)		2.0783(15) × 2		3.3440(3)
	2.0306(15)		2.0795(17) × 2		3.3436(4)
M(2)–O(2)#3	2.080(2)	M(3)–O(6)	2.067(3) × 2	Mo(2)–M(2)#7	3.3678(8)
	2.0813(14)		2.072(2) × 2		3.3658(5)
	2.0823(9)		2.0864(15) × 2		3.3590(3)
	2.0815(11)		2.0881(18) × 2		3.3586(4)
M(2)–O(4)	2.088(3)	M(3)–O(1)	2.134(5)	M(1)–M(1)#2	3.148(4)
	2.0873(19)		2.137(3)		3.149(2)
	2.0767(13)		2.152(2)		3.1453(16)
	2.0738(16)		2.154(2)		3.1428(19)
M(2)–O(3)#4	2.114(3)	M(3)–O(1)#6	2.139(5)	M(2)–M(2)#3	3.1731(14)
	2.1112(19)		2.135(3)		3.1735(8)
	2.1000(13)		2.159(2)		3.1654(5)
	2.0980(15)		2.161(2)		3.1648(6)
M(2)–O(4)#3	2.140(3)	〈M(3)–O〉	2.089	M(2)–M(2)#8	3.2490(14)
	2.1387(19)		2.091		3.2484(8)
	2.1423(13)		2.107		3.2430(6)
	2.1444(15)		2.108		3.2433(6)
M(2)–O(3)#5	2.230(3)			M(3)–M(3)#2	2.5571(3)
	2.2339(19)				2.5552(1)
	2.2426(14)				2.5412(1)
	2.2422(16)				2.5397(1)
〈M(2)–O〉	2.114				
	2.114				
	2.113				
	2.112				

Symmetry codes: #1 x–1, y, z; #2 x–1/2, y, $-z$+1/2; #3 $-x$+1,$-y$+1,$-z$+1; #4 $-x$, y+1/2, $-z$+1; #5 x, $-y$+1/2, z; #6 x+1/2, y, $-z$+1/2; #7 x+1, y, z; #8 $-x$, $-y$+1, $-z$+1.
[a] Correspond to the first, second, third and fourth lines for each distance, respectively.

650 °C and 23 mol% $ZnMoO_4$. The latter values differ from the data by Efremov and Trunov [12] who gave the eutectic point coordinates as 685 °C and 20 mol% $ZnMoO_4$.

In agreement with the authors of [10–14,23–25], we confirmed formation of the single intermediate incongruently melting lithium zinc molybdate, but, in contrast to results of most authors, found it to have a variable composition in a notable range from 66.7 to 76 mol% $ZnMoO_4$. The peritectic point corresponds to 885 °C and 67 mol% $ZnMoO_4$, whereas authors of [12] gave the same composition but the higher temperature, 925 °C. The melting point of the compound increases with growing the x value and reaches the peritectic temperature value at ca. 76–77 mol% $ZnMoO_4$ (Fig. 1). A general outline of the phase diagram resembles T–x diagram of the $MgMoO_4$–$Mg_3V_2O_8$ system where solid solutions $Mg_{2.5+x}V_{1-2x}Mo_{1-2x}O_8$ of the lyonsite-type were found [42].

The dependences of the lattice parameters of the powder samples in the homogeneity range (Table 1, Fig. 2) obey to the Vegard's law. According to the lattice parameter changes in the single- and two-phase regions, the compound has the formula $Li_{2-2x}Zn_{2+x}(MoO_4)_3$, where $0 \le x \le 0.28$ at 600 °C that is in a good agreement with the T–x diagram. An estimated error of the upper x limits is ± 0.01 that corresponding to ca. ± 0.3 mol%. The homogeneity range for lithium zinc molybdate is close to that for $Li_{2-2x}Mg_{2+x}(MoO_4)_3$ ($0 \le x \le 0.3$ at 600 °C) [20] and completely coincides with the homogeneity region found early by us for lithium manganese molybdate [17]. In addition, the course of changing the lattice dimensions for $Li_{2-2x}Zn_{2+x}(MoO_4)_3$ (Fig. 2) is also analogous to those for $Li_{2-2x}M_{2+x}(MoO_4)_3$ (M = Mg, Mn). At the same time our results correct the data obtained by authors of [25] who claimed about $-0.1 \le x \le 0.3$ for the homogeneity range expansion. A negative departure from the stoichiometric formula

Table 5
Bond valence sums for $Li_{2-2x}Zn_{2+x}(MoO_4)_3$ ($x = 0$, 0.03, 0.21 and 0.23)[a].

Atom	Mo(1)	Mo(2)	M(1)	M(2)	M(3)	$\sum s_{ij}$
O(1)	1.546				0.219; 0.216	1.981
	1.537				0.217; 0.216	1.970
	1.556				0.205; 0.200	1.961
	1.559				0.202; 0.198	1.959
O(2)	1.294			0.313 × 2		1.920
	1.309			0.313 × 2		1.935
	1.315			0.313 × 2		1.941
	1.313			0.314 × 2		1.941
O(3)	1.462 (× 2)			0.285; 0.209		1.956
	1.456 (× 2)			0.288; 0.207		1.951
	1.458 (× 2)			0.299; 0.203		1.960
	1.451(× 2)			0.301; 0.203		1.955
O(4)		1.381		0.306; 0.267		1.954
		1.368		0.307; 0.267		1.942
		1.365		0.318; 0.266		1.949
		1.360		0.321; 0.265		1.946
O(5)		1.544	0.173; 0.150 (× 2)			1.867
		1.542	0.172; 0.149 (× 2)			1.863
		1.537	0.173; 0.145 (× 2)			1.855
		1.542	0.173; 0.145 (× 2)			1.860
O(6)		1.477			0.264; 0.262 (× 2)	2.003
		1.480			0.262; 0.258 (× 2)	2.000
		1.493			0.250; 0.245 (× 2)	1.988
		1.492			0.247; 0.241 (× 2)	1.980
O(7)		1.391	0.200 (× 2)	0.355		1.946
		1.388	0.199 (× 2)	0.359		1.946
		1.398	0.200 (× 2)	0.358		1.956
		1.392	0.200 (× 2)	0.361		1.953
$\sum s_{ij}$	5.764	5.793	1.046	1.735	1.487	
	5.758	5.778	1.040	1.741	1.473	
	5.787	5.793	1.036	1.757	1.395	
	5.774	5.786	1.036	1.765	1.376	

Note: Discrepancy factors $D = [(\sum|\sum s_{ij} - v_i|)/\sum v_i]$ after Pyatenko [41] are 2.49%, 2.88%, 2.84% and 2.97% for $x = 0$, 0.03, 0.21 and 0.23, respectively.

[a] Correspond to the first, second, third and fourth lines in each cell, respectively.

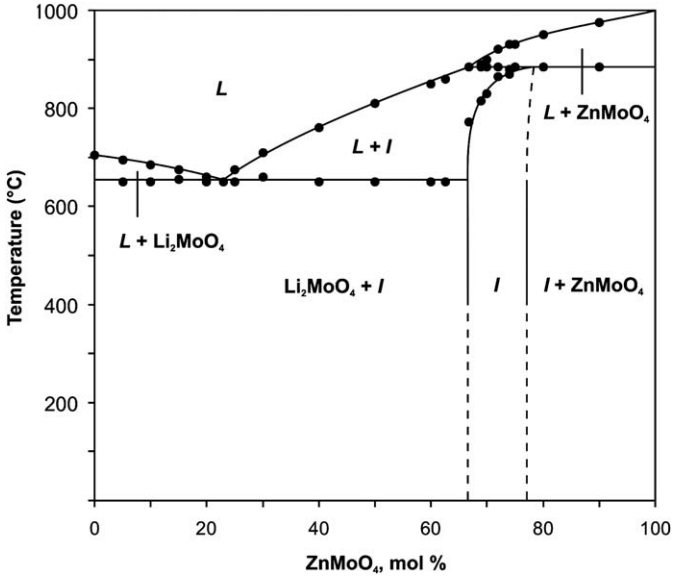

Fig. 1. *T–x* phase diagram of the Li_2MoO_4–$ZnMoO_4$ system: **I**—$Li_{2-2x}Zn_{2+x}(MoO_4)_3$.

($x \leq 0$) results in more than four Li^+ and Zn^{2+}cations per $Li_{2-2x}Zn_{2+x}(MoO_4)_3$ formula unit that required an additional position for arranging the cation excess. It is not confirmed by our and literature data on the lyonsite-type structures [22] and is rather unlikely for samples prepared under conventional conditions. In any case, this demands additional, more thorough data.

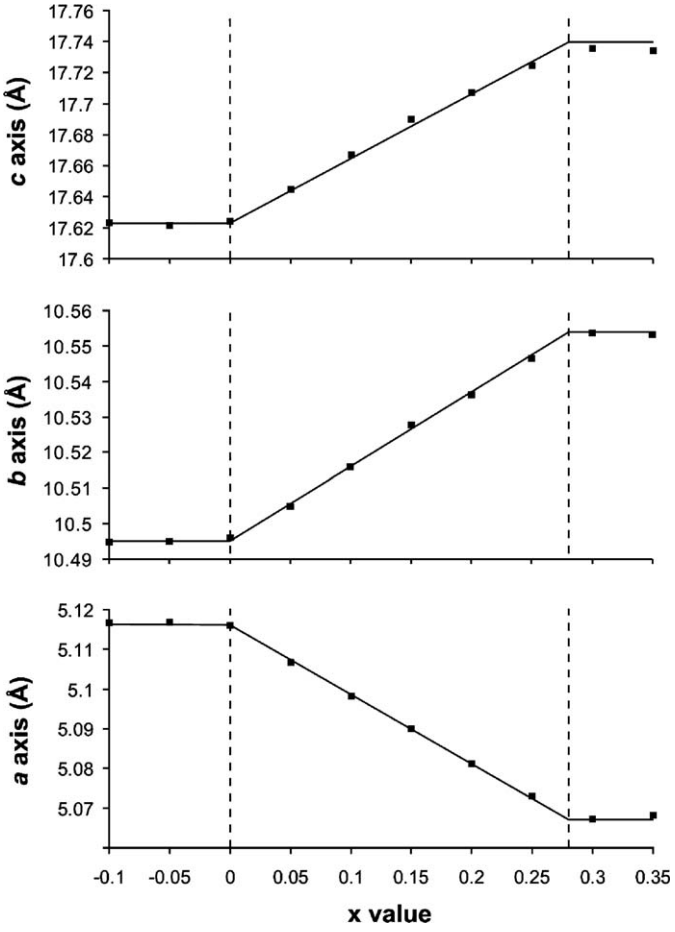

Fig. 2. Dependences of lattice parameters of $Li_{2-2x}Zn_{2+x}(MoO_4)_3$ powder samples on nominal composition. The revealed borders between single- and two-phase regions are shown by dashed lines.

3.2. *Crystal structures of $Li_{2-2x}Zn_{2+x}(MoO_4)_3$ ($x = 0$; 0.03; 0.21 and 0.23)*

In the unit cell of nonstoichiometric lithium zinc molybdate with the general crystal chemical formula $(M1)(M2)_2(M3)(MoO_4)_3$ [16] (the space group *Pnma*, $Z = 4$), there are five kinds of coordination polyhedra, where one of two kinds of MoO_4 tetrahedra, the edge-shared trigonal prismatic *M*1 site and the face-shared octahedral *M*3 site locate on the mirror planes, while the second kind of MoO_4 tetrahedra and the edge/corner-shared octahedral *M*2 site are in the general positions. The linkage patterns of oxygen polyhedra around *M*1, *M*2 and *M*3 sites are given in Fig. 3. The Li^+ and Zn^{2+} cations are statistically distributed over *M*1, *M*2 and *M*3 cation sites; corresponding distributions and the compositions of the studied crystals **I**, **II**, **III** and **IV** have been determined from the crystal structure refinements and listed in Table 3. Accuracy of crystal composition determinations is confirmed by bond valence sum calculations (Table 5). The similar cationic distributions but stoichiometric compositions were found for $Li_2M_2(MoO_4)_3$ (M = Fe, Ni, Cu, Co, Mg) [15,16,18–20] and $Li_2Mg_2(WO_4)_3$ [43]. The lattice parameters, populations of the Li/Zn positions and interatomic distances for the $Li_{1.93}Zn_{2.03}(MoO_4)_3$ (**II**) structure are in a good agreement with the structure data of [25] that indicates to a similar departure of

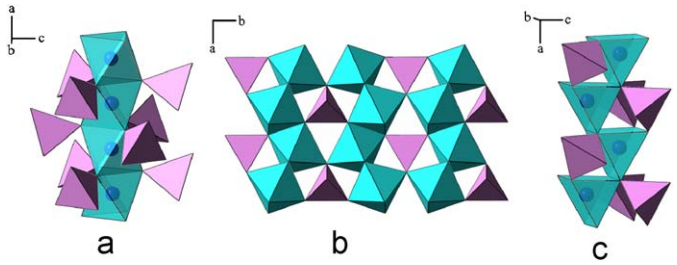

Fig. 3. The linkage patterns of the cationic sites in the $Li_{1.93}Zn_{2.03}(MoO_4)_3$ structure: (a) the zigzag column of edge-sharing $M1O_6$ trigonal prisms with attached $Mo2O_4$ tetrahedra; (b) the lacy wall of edge/corner-sharing $M2O_6$ octahedra with inserted $Mo1O_4$ tetrahedra; and (c) the column of face-sharing $M3O_6$ octahedra with surrounding MoO_4 tetrahedra.

the latter crystal of lithium zinc molybdate from stoichiometry in contrast to the statement of the authors.

In the structures studied, two kinds of crystallographically independent MoO_4 tetrahedra have a normal geometry with close dimensions and average Mo–O distances of 1.772–1.775 Å (Table 4). In the $M1O_6$ trigonal prisms the average $M1$–O bond lengths are 2.176–2.178 Å. Owing to the presence of lithium in the prisms, the $M1$–O bond lengths are slightly greater compared with the Zn–O distances in the similar ZnO_6 prisms in the homeotypic structure of $Zn_{3.77}V_{1.54}Mo_{1.46}O_{12}$ (the space group $P2_12_12_1$, $Z=4$) [39]. The deformed oxygen octahedra around $M2$ and $M3$ sites are somewhat different in size, with the average metal–oxygen bond lengths of 2.112–2.114 and 2.089–2.108 Å, respectively. Despite the insertion of lithium in the both sites, this values are close to the average Zn–O distances found for ZnO_6 octahedra in α-$ZnMoO_4$ [44], $K_2Zn_2(MoO_4)_3$ [45] and $Zn_{3.77}V_{1.54}Mo_{1.46}O_{12}$ [39]. Notice that $M2O_6$ octahedron is larger than $M3O_6$ octahedron, though $M3$ site involves more Li^+ together with vacancies in comparison with $M2$ site. The same phenomenon indicating to a more 'tight' oxygen environment of $M3$ site occurs in isotypical $Li_2Fe_2(MoO_4)_3$ and $Li_3Fe(MoO_4)_3$ [15], $Li_2Ni_2(MoO_4)_3$ [16], $Li_{1.60}Mn_{2.20}(MoO_4)_3$ [17], $Li_2Mg_2(MoO_4)_3$ [20], $Li_3Sc(MoO_4)_3$ [46], and $Mg_{2.54}V_{1.08}Mo_{0.92}O_8$ [42].

The oxygen atoms in the title structure arrange in a manner of the hexagonal closest packing array to form a pseudohexagonal framework with the lacy walls of $M2O_6$ octahedra parallel to (001) and the pinwheels of the isolated MoO_4 tetrahedra with the columns of $M3O_6$ octahedra as the cores (Fig. 4). Note that details of the lyonsite-type structures were repeatedly discussed and described in detail [14,15,21,47] and there is no need to do this again. However, we would like to emphasize that the columns (Fig. 2(c)) are likely the most unstable part of the structure because of the extremely short distances between the adjacent $M3$ sites (2.540–2.557 Å). The steric strain can be partly relieved by incorporation of defects into this site that results in nonstoichiometry of lithium zinc molybdate as well as $Li_{2-2x}M_{2+x}(MoO_4)_3$ (M = Mn, Mg) [17,20] and other related compounds.

The most interesting is to consider changes of $Li_{2-2x}Zn_{2+x}(MoO_4)_3$ structure in dependence on the composition. Notice that such investigation was performed for lyonsite-type compounds for the first time. Primarily, we would like to mark that the unit cell dimensions of the crystals (Table 2) are in a reasonable agreement with the dependence of the lattice parameters on composition measured on powdered samples (Table 1). Slight discrepancies could be explained by a difference in sample preparation conditions: the crystallization temperatures were about 200–300 °C higher than the temperatures of solid state synthesis. It is of considerable interest to consider cationic distribution over $M1$, $M2$ and $M3$ positions on the crystal

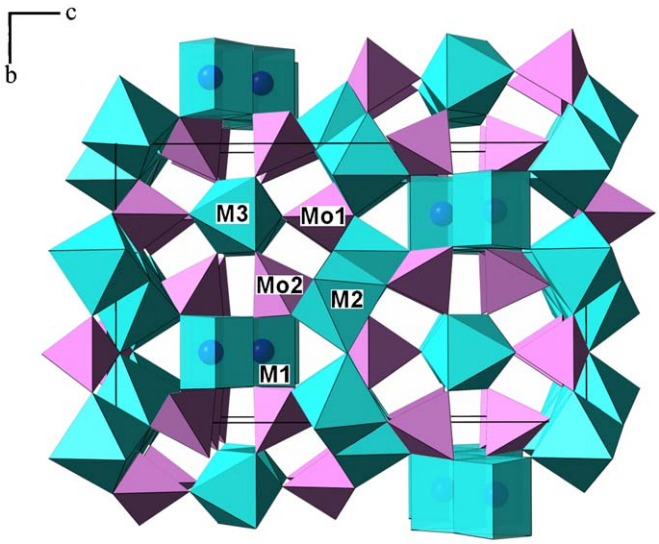

Fig. 4. General view of $Li_{1.93}Zn_{2.03}(MoO_4)_3$ structure along the [100] direction.

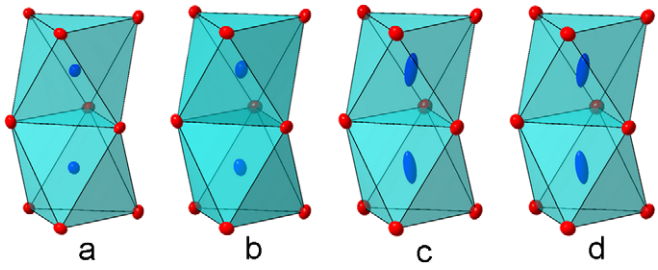

Fig. 5. Change of thermal ellipsoid shapes for atoms in $M3$ site in $Li_{2-2x}Zn_{2+x}(MoO_4)_3$ structure in dependence of composition: (a) $x=0$; (b) $x=0.03$; (c) $x=0.21$; and (d) $x=0.23$.

composition and environment of $M3$ site in the structures determined. In contrast to $M1$ and $M2$ sites with the approximately constant cationic content, $M3$ position changes its content remarkably and is mainly responsible for a departure of lithium zinc molybdate from stoichiometry according to the scheme $2Li^+ \rightarrow Zn^{2+} + \square$ (Table 3). In accordance with this feature of $M3$ site, the average $M3$–O distance increases markedly (from 2.089 Å for $x=0$ up to 2.109 Å for $x=0.23$) while the mean $M1$–O and $M2$–O bond lengths are practically invariable. Cationic vacancies in $M3$ site decrease the amount of the short contacts $M3$–$M3$ and give facilities for the cations in $M3$ to shift towards vacancies in the adjacent $M3$ positions. Such displacement presumably influences the shape of the thermal ellipsoid of $M3$, which becomes more and more elongated along the axis of $M3O_6$ octahedra column with growing the content of vacancies in this site (Fig. 5). Similar anisotropy of thermal vibrations of the cations in $M3$ position was observed in other lyonsite-type structures such as $NaCo_{2.31}(MoO_4)_3$ [47], $Cu_{4-x}Mo_3O_{12}$ ($x \approx 0.15$) [29] $Li_{1.60}Mn_{2.20}(MoO_4)_3$ [17], $(Cu, Mn)_{3.66}Mo_3O_{12}$ [34], $Zn_{3.77}V_{1.54}Mo_{1.46}O_{12}$ [39], $Co_4Fe_{3.33}(VO_4)_6$ and $Mn_3Fe_4(VO_4)_6$ [48] that we could surely consider as a characteristic feature of defects presence in this site. The more vacancies in $M3$ sites, the more the structure expands in the (100) plane and contracts in the [100] direction (Tables 1 and 2, Fig. 2). This is also accounted for an influence of $M3$ position population: increasing content of vacancies results in a compression of $M3O_6$ octahedron along the a axis and its expansion in the directions of the b- and c-axes (Table 4). The same phenomenon also occurs for $Li_{2-2x}M_{2+x}(MoO_4)_3$ (M = Mn, Mg) [17,20].

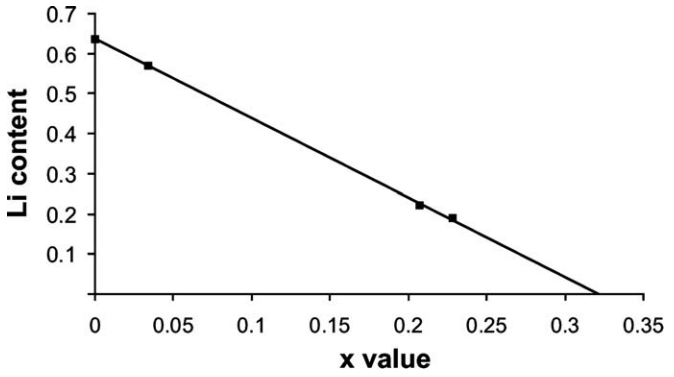

Fig. 6. Dependence of lithium content in *M*3 site on the *x* value in $Li_{2-2x}Zn_{2+x}(MoO_4)_3$ structure.

The fact is claiming attention that the lithium content in *M*3 site decreases almost linearly with the *x* growing (Fig. 6) according to the mentioned substitution/subtraction scheme $2Li^+ \rightarrow Zn^{2+}+\square$. Extrapolation of this dependence to zero lithium concentration gives $x \approx 0.32$ that is slightly greater than $x = 0.28$ found from powder XRD data and witnesses about possible expansion of the homogeneity region at higher temperatures. Hence, we can conclude that the upper *x* limit for $Li_{2-2x}Zn_{2+x}(MoO_4)_3$ is connected with the complete disappearance of lithium in *M*3 position. Analogous reason of homogeneity range termination would be expected for other double molybdates $Li_{2-2x}M_{2+x}(MoO_4)_3$ (M = Mg, Mn, Co, Ni, Cu).

The most likely, the deficiency of *M*3 sites is a general feature of the structure type and its relatives and is caused by steric strains in the face-sharing columns of $M3O_6$ octahedra (Fig. 2(c)). It should be noted that our experimental data on $Li_{2-2x}M_{2+x}(MoO_4)_3$ (M = Mn, Zn) and the present discussion raise the question of revising the compositions of isostructural double molybdates $Li_3M(MoO_4)_3$, where M^{3+} = Al, Ga, Cr, Fe, Sc, In [13,46,49–51], which would be deviated from the stoichiometry in accordance with the expected general formula $Li_{3-3x}M_{1+x}(MoO_4)_3$.

3.3. Crystal growth of lithium zinc molybdate

Lithium zinc molybdate crystals grown by spontaneous crystallization have the shape of well-faceted colorless pseudo-hexagonal prisms elongated in the [100] direction and with the sizes reaching up to 0.5 mm wide and 5 mm long. The most expressed prismatic faces of the crystals are {010} and {013}. The largest good-quality crystals grew from nonstoichiometric melts of the Li_2MoO_4–$ZnMoO_4$ system in the range about 70–75 mol% of $ZnMoO_4$.

The results of studying *T*–*x* phase diagram of the Li_2MoO_4–$ZnMoO_4$ system, determination of the crystal structure of lithium zinc molybdate and its spontaneous crystallization from different melts were used for growing large crystals of the double molybdate by the Czochralski technique under low-temperature gradients [35]. Optically homogeneous crystals with the composition close to the stoichiometric formula were grown on seeds oriented along [100] and [010] (Fig. 7(a) and (b)). Coloration of the crystals grown with using commercially available Li_2CO_3, ZnO and MoO_3 (all analytical grade) was practically disappeared after additional purification of MoO_3 (Fig. 7(c)). Maximum sizes of the crystals reach $30 \times 40\,mm^2$ in the cross-section and up to 75 mm in length. The material is nonhygroscopic and chemically resistant. As-grown undoped crystals of a good optical quality were further used for physical measurements. As a next step we intend to grow $Li_2Zn_2(MoO_4)_3$ crystals from raw materials with an ultra-low radioactive background.

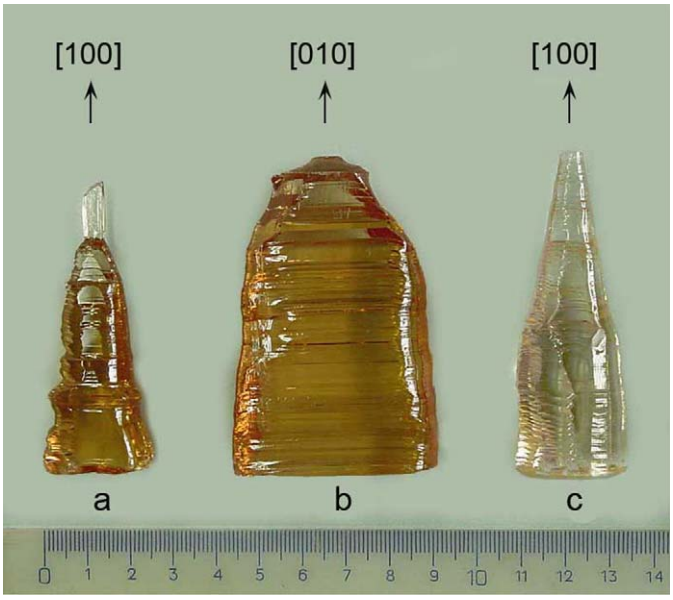

Fig. 7. Large crystals of lithium zinc molybdates grown using the low-thermal-gradient Czochralski technique under different conditions: (a) crystals pulled in [100] direction; (b) crystals pulled in [010] direction; and (c) crystals pulled in [100] direction using purified MoO_3.

3.4. Physical properties

The preliminary results of studying physical properties of $Li_2Zn_2(MoO_4)_3$ crystals were described in [52]. Measurements of optical properties of the as-grown crystals showed them to be biaxial and have the refractive indexes 1.98–2.02 in the radiation region of 580–435 nm. An additional purification of raw materials decreases absorption in the crystal, which allows concluding that further purification could improve optical properties of the material. Excitation and reflectivity spectra under UV, synchrotron and X-ray radiation were measured in the temperature interval 10–300 K. Exciting the crystals with radiation at $E_{ex} = 4.0$ eV gives a broad luminescence band with maximum at 2.02 eV. Luminescence intensity increases with a decrease of the temperature. Scintillation properties of $Li_2Zn_2(MoO_4)_3$ were tested with α particles of ^{241}Am source. The photoelectron yield of lithium zinc molybdate was estimated as ~4% of $CaMoO_4$ at 220 K. Applicability of the crystals as cryogenic low-temperature detectors were demonstrated for the first time. Despite the scintillation properties of $Li_2Zn_2(MoO_4)_3$ crystals are rather poor, the material can be used as a bolometric detector to search for 2β decay of ^{100}Mo. EPR studies of $Li_2Zn_2(MoO_4)_3$ crystals [53] show that scintillating properties are provoked by Cu^{2+} impurities substituting Zn^{2+} cations mainly in *M*2 site. The Cu^{2+} cations are in $3d^9$ state with electronic spin $S = \frac{1}{2}$ and EPR spectra are described by the following spin Hamiltonian parameters: $g_{||} = 2.38$, $g_{\perp} = 2.06$, $A_{||} = 116$ Gs, $A_{\perp} = 0$ Gs. The directions of the main values of *g* and *A* tensors (g_{zz} and A_{zz}) correspond to a O–Cu–O direction of the CuO_6 distorted octahedron. The detailed physical measurements data will be published in forthcoming papers.

Acknowledgments

The authors are grateful to Dr. Dmitry Yu. Naumov and Dr. Natalia V. Kuratieva for collecting and processing X-ray single-

crystal diffraction data on a Bruker-Nonius X8 Apex CCD diffractometer. This work was partly supported by the Russian Foundation for Basic Research, Grant 03-08-00384.

Appendix A. Supplementary material

Supplementary data associated with this article can be found in the online version at doi:10.1016/j.jssc.2009.04.036.

References

[1] A.A. Kaminskii, Laser Crystals, their Physics and Properties, second ed., Springer Series in Optical Sciences, vol. 14, Springer, Berlin, Germany, 1990.
[2] M. Globus, B. Grinyov, J.K. Kim, Inorganic Scintillators for Modern and Traditional Applications, Kharkiv, 2005.
[3] F.T. Avignone III, G.S. King III, Yu.G. Zdesenko, New J. Phys. 7 (2005) 1–46.
[4] G. Audi, A.H. Wapstra, C. Thibault, Nucl. Phys. A 729 (2003) 337–746.
[5] Yu.G. Zdesenko, B.N. Kropivyanskii, V.N. Kuts, A.S. Nikolaiko, V.T. Gabrielyan, S.V. Akimov, Instrum. Exp. Tech. 39 (1996) 362–366.
[6] V.B. Mikhailik, H. Kraus, D. Wahl, M.S. Mykhaylyk, Phys. Stat. Sol. B 242 (2005) R17–R19.
[7] V.B. Mikhailik, H. Kraus, D. Wahl, H. Ehrenberg, M.S. Mykhaylyk, Nucl. Instrum. Meth. A 562 (2006) 513–516.
[8] O.P. Barinova, S.V. Kirsanova, S. Pirro, F.A. Danevich, S.S. Nagorny, in: Abstracts of National Conference on Crystal Growing (NCCG 2006), Moscow, October 23–27, 2006, p. 280.
[9] L.N. Demyanets, Kristallografiya 14 (1969) 955–958.
[10] V.A. Efremov, V.K. Trunov, Z. Neorg. Khim. 17 (1972) 2034–2039.
[11] C. Gicquel, C. Mayer, G. Pezez, R. Bouaziz, C. R. Acad. Sci. C 275 (1972) 265–267.
[12] V.A. Efremov, V.K. Trunov, Z. Neorg. Khim. 20 (1975) 2200–2203.
[13] V.A. Efremov, V.K. Trunov, Izv. AN SSSR Neorg. Mater. 11 (1975) 273–277.
[14] V.G. Penkova, P.V. Klevtsov, Z. Neorg. Khim. 22 (1977) 1713–1715.
[15] R.F. Klevtsova, S.A. Magarill, Kristallografiya 15 (1970) 710–715.
[16] M. Ozima, S. Sato, T. Zoltai, Acta Crystallogr. B 33 (1977) 2175–2181.
[17] S.F. Solodovnikov, Z.A. Solodovnikova, R.F. Klevtsova, L.A. Glinskaya, P.V. Klevtsov, E.S. Zolotova, J. Struct. Chem. (1994) 871–878.
[18] M. Wiesmann, M. Geselle, H. Weitzel, H. Fuess, Z. Kristallogr. 209 (1995) 615.
[19] M. Wiesmann, I. Svoboda, H. Weitzel, H. Fuess, Z. Kristallogr. 210 (1995) 525.
[20] L. Sebastian, Y. Piffard, A.K. Shukla, F. Taulelle, J. Gopalakrishnan, J. Mater. Chem. 13 (2003) 1797–1802.
[21] J.M. Hughes, S.J. Starkey, M.L. Malinconico, L.L. Malinconico, Am. Miner. 72 (1987) 1000–1005.
[22] J.P. Smith, P.C. Stair, K.R. Poeppelmeier, Chem. Eur. J. 12 (2006) 5944–5953.
[23] L. Xue, Z. Lin, F. Huang, J. Liang, Chin. J. Struct. Chem. 26 (2007) 1208–1210.
[24] L. Xue, D. Chen, Z. Lin, P. Lv, F. Huang, J. Liang, J. Alloys Compd. 430 (2007) 67–70.
[25] L. Xue, Y. Wang, P. Lv, D. Chen, Z. Lin, J. Liang, F. Huang, Z. Xie, Cryst. Growth Des. 9 (2009) 914–920.
[26] S.F. Solodovnikov, D.Sc. Chemistry, Thesis, Institute of Inorganic Chemistry, SB RAS, Novosibirsk, Russia, 2000.
[27] S.F. Solodovnikov, Z.A. Solodovnikova, A.A. Pavlyuk, E.S. Zolotova, L.I. Yudanova, in: Proceedings of the First Russian–German Seminar on Thermodynamics and Materials Science, Novosibirsk, September 23–25, 2008, p. 90.
[28] V.A. Efremov, Yu.G. Petrosyan, V.M. Zhukovsky, Z. Neorg. Khim. 22 (1977) 175–179.
[29] L. Katz, A. Kasenally, L. Kihlborg, Acta Crystallogr. B27 (1971) 2071–2077.
[30] U. Steiner, W. Reicchelt, H. Oppermann, Z. Anorg. Allg. Chem. 622 (1996) 1428–1434.
[31] H. Szillat, H.K. Müller-Bushbaum, Z. Naturforsch. 50b (1995) 247–251.
[32] H. Szillat, H.K. Müller-Bushbaum, Z. Naturforsch. 50b (1995) 707–711.
[33] O. Sedello, H.K. Müller-Bushbaum, Z. Naturforsch. 51b (1996) 90–94.
[34] O. Sedello, H.K. Müller-Bushbaum, Z. Naturforsch. 51b (1996) 447–449.
[35] A.A. Pavlyuk, Ya.V. Vasiliev, L.Yu. Kharchenko, F.A. Kuznetsov, in: Proceedings of the Asia Pacific Society for Advanced Materials APSAM-92, April 26–29, 1992, Shanghai, 1993, p. 164.
[36] B.H. Toby, J. Appl. Cryst. 34 (2001) 210–213.
[37] SAINT (Version 7.03), SADABS (Version 2.11), Bruker AXS Inc., Madison, Wisconsin, 2004.
[38] G.M. Sheldrick, SHELX-97, University of Göttingen, Germany, 1997.
[39] X. Wang, K.R. Heier, C.L. Stern, K.R. Poeppelmeier, J. Alloys Compd. 255 (1996) 190–194.
[40] I.D. Brown, D. Altermatt, Acta Crystallogr. B41 (1985) 244–247.
[41] Yu.A. Pyatenko, Kristallografiya 17 (1972) 773–779.
[42] X. Wang, C.L. Stern, K.R. Poeppelmeier, J. Alloys Compd. 243 (1996) 51–58.
[43] Z. Fu, W. Li, Powder Diffr. 9 (1994) 158–160.
[44] S.C. Abrahams, J. Chem. Phys. 46 (1967) 2052–2063.
[45] C. Gicquel-Mayer, G. Perez, Rev. Chim. Miner. 12 (1975) 537–545.
[46] U. Kolitsch, E. Tillmans, Acta Crystallogr. E59 (2003) i55–i58.
[47] J.A. Ibers, G.W. Smith, Acta Crystallogr. 17 (1964) 190–197.
[48] X. Wang, D.A. Griend, C.L. Stern, K.R. Poeppelmeier, Inorg. Chem. 39 (2000) 136–140.
[49] P.V. Klevtsov, Kristallografiya 15 (1970) 797–802.
[50] V.K. Trunov, V.A. Efremov, Z. Neorg. Khim. 16 (1971) 2026–2027.
[51] A. van der Lee, M. Beaurain, P. Armand, Acta Crystallogr. C C64 (2008) i1–i4.
[52] N.V. Bashmakova, F.A. Danevich, V.Ya. Degoda, I.M. Dmitruk, S.Yu. Kutovoi, V.M. Mokina, S.S. Nagorny, S. Nisi, A.S. Nikolaiko, A.A. Pavlyuk, S. Pirro, A.E. Savon, D.A. Spassky, S.F. Solodovnikov, Z.A. Solodovnikova, V.I. Tretyak, S.M. Vatnik, E.S. Zolotova, in: International Conference on Engineering of Scintillator Materials and Radiation Technology (ISMART-2008), November 17–21, 2008, Kharkiv, Ukraine, p. 34.
[53] V.A. Nadolinny, N.V. Cherney, A.V. Sinitsyn, A.A. Pavlyuk, S.F. Solodovnikov, Z. Strukt. Khim. 49 (2008) 891–895.